Bioelectrochemistry 152 (2023) 108461

Contents lists available at ScienceDirect

Bioelectrochemistry

journal homepage: www.journals.elsevier.com/bioelectrochemistry

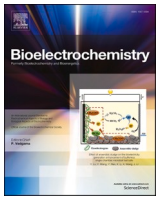

Development of a novel electrochemical biosensor based on plastic antibodies for detection of STEAP1 biomarker in cancer

Margarida Carvalho [a,b,c,d], Rui M. Gomes [a,b,i], Sandra Moreira Rocha [c], Jorge Barroca-Ferreira [c,d,e], Claudio J. Maia [c], Lucía Guillade [g,h], Miguel A. Correa-Duarte [g,h], Luís A. Passarinha [c,d,e,f], Felismina T.C. Moreira [a,b,*]

[a] BioMark Sensor Research/ISEP, School of Engineering, Polytechnic Institute, Porto, Portugal
[b] CEB, Centre of Biological Engineering, Minho University, Braga, Portugal
[c] CICS-UBI-Health Science Research Centre, University of Beira Interior, Av. Infante D. Henrique, 6200-506 Covilha, Portugal
[d] Associate Laboratory i4HB-Institute for Health and Bioeconomy, Faculdade de Ciências e Tecnologia, Universidade NOVA de Lisboa, 2819-516 Caparica, Portugal
[e] UCIBIO-Applied Molecular Biosciences Unit, Departamento de Química, Faculdade de Ciências e Tecnologia, Universidade NOVA de Lisboa, 2829-516 Caparica, Portugal
[f] Laboratório de Fármaco-Toxicologia-UBIMedical, Universidade da Beira Interior, 6200-284 Covilha, Portugal
[g] CINBIO, Universidade de Vigo, 36310 Vigo, Spain
[h] Center for Biomedical Research (CINBIO), Southern Galicia Institute of Health Research (IISGS), and Biomedical Research Networking Center for Mental Health (CIBERSAM), Spain
[i] Faculty of Engineering, Porto University, Portugal

ARTICLE INFO

Keywords:
Prostate cancer
Biosensor
STEAP1
Molecularly imprinted polymers

ABSTRACT

STEAP1 is a cell surface protein of the STEAP family whose main function focuses on intercellular communication and cell growth. STEAP1 is considered a promising putative biomarker and a candidate target for prostate cancer treatment.

For specific and selective detection of STEAP1, a molecularly imprinted polymers (MIP) was developed on a screen-printed electrode (C-SPE) whose surface was modified with a nanocomposite based on carbon nanotubes decorated with dendritic platinum nanoparticles (CNTs- PAH /Pt). Then, the MIPs were produced on the modified C-SPE by electropolymerization of a mixture of STEAP1 and a monomer (pyrrole-2-carboxylic acid). Then, the protein was removed from the polymeric network by enzymatic treatment with trypsin, which created the specific template cavities for further STEAP1 detection. Electrochemical techniques such as EIS and CV were used to follow the chemical modification steps of C-SPE. The analytical performance of the biosensor was evaluated by SWV in PBS buffer and in lysates of neoplastic prostate cancer cells (LNCaP) extracts. The MIP material showing a linear range from 130 pg/ml to 13 μg/ml. Overall, the biosensor exhibits essential properties such as selectivity, sensitivity and reproducibility for its application in medical and clinical research diagnosis and/or prognosis of prostate cancer.

1. Introduction

Prostate cancer (PCa) is the most established cancer in men worldwide [1]. The main challenge is to diagnose it at an early stage so that we can control the disease to some extent to ensure patient survival and quality of life [2,3]. So, there is an urgent need for alternative and innovative methodologies in the identification and targeting of novel and relevant biomarkers in PCa. Six-Transmembrane Epithelial Antigens of the Prostate (STEAP) proteins are a family with functions in cell proliferation and oxidative stress, which are associated with cancer progression [4,5]. Specifically, The Six-Transmembrane Epithelial Antigen of the Prostate 1 (STEAP1) is a membrane protein overexpressed in PCa, being mostly absent from other tissues or vital organs [5]. Due to the predominantly α-helical secondary structure, localization at the cell surface in tight- and gap-junctions and the intracellular disposition of both C- and N- terminal, it has been suggested that STEAP1 functions as a transmembrane channel, transporting ions and small molecules, while also playing a role in cell adhesion and intercellular communication

* Corresponding author at: BioMark Sensor Research/ISEP, School of Engineering, Polytechnic Institute, Porto, Portugal.
E-mail address: ftm@isep.ipp.pt (F.T.C. Moreira).

https://doi.org/10.1016/j.bioelechem.2023.108461
Received 15 February 2023; Received in revised form 1 May 2023; Accepted 5 May 2023
Available online 9 May 2023

[6,7,8]. According to Barroca-Ferreira and coworkers, STEAP1 levels are higher in malignant tissue than in healthy tissue, and these levels may be associated with a particularly aggressive stage of the disease, noting that STEAP1 can be used for PCa prognosis and diagnosis [9,10,11]. Although there is no demonstration that STEAP1 is secreted by cells, there is evidence for its presence in extracellular fluids. However, the physiological levels of STEAP1 in prostate cancer patients are not yet known [7,8]. Thus, the detection and quantification of STEAP1 is essential in the diagnosis of PCa, due to the fact that its expression is practically limited to prostate tissue [12]. Indeed, STEAP1 overexpression has been suggested to be a driving force for PCa initiation and progression, enhancing tumor proliferation and aggressiveness, rendering it an attractive PCa biomarker and therapeutic target. Concurrently, STEAP1 also appears to distinguish between BPH and prostatic intraepithelial neoplasia, meaning that PCa can be diagnosed and treated before adenocarcinoma progression, while avoiding the high false-positive rate of PSA [3,9,13]. Several methods have been described in the literature for the detection and quantification of various biomarkers associated with PCa, including optical, separation, and biochemical approaches [9,10,11]. However, the high cost and cycle time as well as low reproducibility and efficiency are some of the major drawbacks. Therefore, as an emerging technology, biosensors can rapidly and accurately detect a biomarker [14].

There are a lot of different available biosensors for biomarkers detection, like optical, enzymatic, and electrochemical biosensors [13,14,15]. Since the goal of this work is to detect a protein, a highly specific biological recognition element must be found to enable its detection in a complex medium such as biological samples. Natural biological recognition elements such as enzymes, antibodies, and proteins are not only expensive, but also exhibit low stability and durability under certain conditions despite their good selectivity and affinity for the target [16]. Therefore, synthetic biological recognition elements such as molecular imprinting polymers (MIPs) seem to be the best option because this emerging technology is cheap, simple, and has high specificity and selectivity for the target [17,18].

Electrochemical biosensors have received special attention due to their high stability, reproducibility, sensitivity, and low cost [19]. Since this type of biosensor requires an electron transfer phenomenon, the polymerization of the monomer such as pyrrole-2-carboxylic acid (PY-COOH) could form a polymeric matrix through electropolymerization, which facilitates current passage and makes the biosensor more sensitive to surface changes [20]. Several works are described in the literature focusing on the synthesis of MIPs for the detection of other biomolecules associated with inflammatory diseases such as Alzheimer's disease and cancer, where (PY-COOH) and Py. Gonçalves and co-workers describe the development of an electrochemical biosensor for the determination of interleukin-6 using screen-printed carbon electrodes (C-SPE) as a support for the construction of a MIP with Py as a monomer for the detection of interleukin-6 [21]. In addition, Gomes and coworkers described the development of a MIP material based on the electropolymerization of Py and Py-COOH for the detection of cystain C, a protein associated with chronic kidney disease, also using C-SPE [22]. In this work, the team used carbon nanotubes in the polymer matrix to achieve the desired sensitivity. Moreira and coworkers have reported work using PY to develop MIPs for the detection of CEA, a cancer biomarker. The device showed good analytical performance using silver electrodes as the support material. The electrodes were subjected to electrochemical oxidation to obtain stable readings [23]. Here, we improved the literature by combining PY-COOH with a nanocomposite of dendritic platinum nanoparticles aminated with carbon nanotubes (CNTs- PAH /Pt). In the presence of STEAP1, this leads to a stable polymer matrix on the C-SPE surface due to the interaction between the amine groups of the composite and the carboxyl groups of the protein through hydrogen bonds and electrostatic interactions. Overall, the incorporation of a composite such as CNTs- PAH /Pt, which are highly conductive, not only makes the biosensor more sensitive, but could form a complex between STEAP1 and the polymer due to its amine group [24]. Specifically, the carboxyl group of PY-COOH binds to the amino group of STEAP1 via non-covalent bonds, and the amino group of CNTs PAH /Pt binds to the carboxylic group of PY-COOH, forming a highly conductive and stable complex between these elements. M. E. Schneider and coworkers described a similar nanomaterial to platinum nanoparticle-coated aminated carbon nanotubes (MWCNTs- PAH /Pt) for the development of an immunosensor to detect a biomarker associated with Alzheimer's disease [25].

Therefore, the aim of the present work is to develop for the first time an electrochemical biosensor for the detection of STEAP1 using the technology of molecular imprinting of the protein in combination with a conductive polymer (PY-COOH) and an innovative composite of CNTs/PAH-Ptd. The MIP biosensor was optimized and characterized, as well as its performance in the detection phase of STEAP1.

2. Experimental section

2.1. Material and equipment's

Electrochemical procedures were performed on a Metrohm Autolab Potentiostat/Galvanostat (controlled by Nova 2.1. software) using a conductive box DropSens (DRP-DSC). The C-SPE electrodes were purchased from DropSens (DRP-C110) and consisted of a silver reference electrode, a carbon auxiliary electrode, and a carbon working electrode (4 mm diameter). Raman spectroscopy was used to record the chemical analysis of the biosensor in a Thermo Scientific DXR RAMAN with a 532 nm confocal excitation laser.

Surface morphology of the various samples was determined using a field emission scanning electron microscope (FESEM, JEOL-JSM 6700F) equipped with a retractable backscattered electron detector and an Oxford Inca EDX system detector for compositional analysis. Another technique for morphology analysis was the transmission electron microscope (TEM, JEOL-JEM 1010) with an accelerating voltage of 100 kV. High-resolution transmission electron microscopy (HRTEM) was performed with a microscope (JEOL-JEM 2010F) at 200 kV (accelerating voltage).

2.2. Reagents and solutions

Phosphate-buffered saline (PBS) was purchased from VWR and used to prepare all other solutions. Potassium ferricyanide III ($K_3[Fe(CN)_6]$) and potassium ferricyanide II ($K_4[Fe(CN)_6]$) were purchased from Riedel-de-Haen. Potassium chloride (KCl) and oxalic acid were purchased from Merck. Pyrrole-2-carboxylic acid was purchased from Alfa Aesar.

For electrochemical measurements, a redox probe was prepared with a equimolar solution of $K_3[Fe(CN)_6]$ and $K_4[Fe(CN)_6]$ ($[Fe(CN)_6]^{3-/4-}$) at a concentration of 5.0×10^{-3} M in PBS buffer. For selectivity studies, some interfering species such as carcinoembryonic antigen (CEA) (0.25 ng/ml), aminobenzoic acid (0.11 μg/ml), and l-glutamic acid (2.22 μg/ml) contained in 10-fold diluted pellet of LNCaP cellular extracts were used.

2.3. Cell culture

The LNCaP prostate cancer cell line was purchased from the European Collection of Cell Cultures (ECACC, UK) and maintained in RPMI 1640 medium (Sigma-Aldrich Co. St. Louis, MO, USA), supplemented with 10% fetal bovine serum (FBS) (Biochrom AG, Berlin, Germany) and 1% penicillin/streptomycin (ThermoFisher Scientific, Waltham, MA, USA), in a humidified chamber at 37 °C and a 5% CO_2 atmosphere. LNCaP cells have grown in 75 cm^2 t-flasks (n = 6) until 80–90% confluence. Cells were trypsinized, washed and diluted 10 times in PBS.

2.4. Electrochemical procedures

The electrochemical techniques under this work were electrochemical impedance techniques (EIS), cyclic voltammetry (CV), square wave voltammetry (SWV), and chronoamperometry (CA). The electrodes pre-treatment was performed by CA for electrode activation and cleaning with KCl at a potential of 1.7 V for 200 s.

All electrochemical tests were performed using the redox probe reaction 5 mM $[Fe(CN)_6]^{3-/4-}$ in 0.1 M KCl, which induces an electron transfer process at the C-SPE surface and allows characterization of the surface by techniques such as CV and EIS. In these experiments, CV was scanned within a potential of − 0.6 to + 0.6 V at 0.050 V/s. The EIS was performed with $[Fe(CN)_6]^{3-/4-}$ solution in open circuit (OCP) using a sinusoidal potential perturbation with an amplitude of 0.1 V over a frequency range of 0.1 to 100 kHz. These techniques were used to control the modification of the electrode surface.

The electropolymerization of the polymers was performed by CV with a scan rate of 0.02 V/s and a potential between − 0.8 and 1.1 V. Electrochemical treatment with PBS after removal of trypsin from the sensor surface was performed by CV with a scan rate of 0.05 V/s and a potential between − 0.4 and 0.5 V.

Calibration curves were performed in PBS buffer and in spiked LNCaP cell culture with STEAP1 ranging from 130 pg/mL to 13 μg/mL. SWV results were fitted within a potential between − 0.1 and 0.5 V and a scan rate of 0.02 V/s using commercial software NOVA to generate the calibration curve. Increasing concentrations of STEAP1 were added to PBS and a pellet of LNCaP cellular extracts. Each concentration was incubated on the sensor surface for 20 min. The data obtained was read with the redox probe $[Fe(CN)_6]^{3-/4-}$ and used to construct the calibration curve. Selectivity tests were performed by mixing different interference species with STEAP1 in PBS buffer pH 7.4. All data was obtained in triplicate using the software NOVA.

2.5. Synthesis of CNTs-PAH/Pt

The first step in the synthesis of the composite was the functionalization of carbon nanotubes (CNTs) with (poly)electrolytes. For this purpose, multi-walled CNTs (CNTs, Nanolab, 5–20 μm long and 10–15 nm in diameter) were sonicated in an acetone/EtOH mixture (1:1, 20 mL) for 10 min and then centrifuged three times (9000 rpm, 20 min), followed by redispersion in ultrapure water (18 MΩ cm^{-1}). After this process, the resulting sample was freeze-dried for 48 h and then used without further treatment. In the next step, the CNTs (7.5 mg) were dispersed in an aqueous solution of 0.5-M NaCl (50 mL) containing 1 wt % polyalamine hydrochloride (PAH), resulting in a final concentration of 150 mg/L. To achieve coating of the CNTs by PAH, the pH of the resulting solution was adjusted to 9.5. The resulting solution of CNTs with PAH was magnetically stirred and then sonicated with an ultrasonic probe for 3 h to ensure that dispersion occurred. To remove the excess of PAH in the solution, 3 cycles of centrifugation (12000 rpm, 24 h) were performed, followed by redispersion by sonication in water. After measuring the absorbance and generating a calibration curve, the concentration of CNTs was determined to be 0.6 mg/mL. For the synthesis of platinum dendritic nanoparticles (Ptd-NPs), $NaBH_4$ (1.22 mL, 0.015 M) was rapidly injected into a mixture of sodium citrate tribasic dihydrate (1.25 mL, 0.1 M) and K_2PtCl_4 (1.25 mL, 0.1 M) in H_2O (21.52 mL) at 800 rpm. The resulting mixture was stirred for 10 min and used immediately. $NaBH_4$ (1.22 mL, 0.015 M) was rapidly injected into a mixture of sodium citrate tribasic dihydrate (1.25 mL, 0.1 M) and K_2PtCl_4 (1.25 mL, 0.1 M) in H_2O (21.52 mL) at 800 rpm. The resulting mixture was stirred for 10 min and used immediately. For the deposition of CNTs, 20 μl of previously synthesized CNTs-PAH (0.6 mg/mL) were added to the Ptd-NPs mixture (10 mL. 4.95 M), and the mixture was then stirred for 30 min. Finally, the resulting dispersion was centrifuged at 9000 rpm for 10 min (procedure repeated 2 times) and redispersed in 5 mL of H_2O at a concentration of 0.0024 mg/mL of CNTs.

2.6. Biosensing SETUP

For the biosensor design, the C-SPE was first subjected to electrochemical activation with a 0.1 M KCl solution, applying 1.7 V for 200 s using the technique CA (Fig. 1A). Then, 5 μl of CNTs-PAH/Pt nanocomposite was drop casted on top of the C-SPE surface and subsequently incubated at 60 °C for 20 min (Fig. 1B). For the electropolymerization step of the MIP, a bulk solution containing 10% STEAP1 (0.1 μg/ml), 20% PY-COOH (0.01 M), and 70% PBS was performed using the CV technique for 10 cycles with a potential range between − 0.8 and 1.1 V at a scan rate of 0.02 V/s. For the NIP material, the only difference was the absence of the STEAP1 in the polymeric solution, so the ratio was 20% PY-COOH (0.01 M) and 80% PBS (Fig. 1C). Finally, the STEAP1 removal step was performed by dropping 5 μl of 100-fold diluted trypsin onto the modified C-SPE containing the MIP and NIP polymers and incubating at 37 °C for 1 h, followed by a electrochemical procedure with PBS in order to remove amino acids or unreacted monomers of the electrodes surface, by CV during 10 cycles with a potential between − 0.4 and 0.5 V at a scan rate of 0.05 V/s (Fig. 1D).

3. Results and discussion

3.1. Biosensing SETUP

Electrochemical control of C-SPE modification was achieved by EIS and CV techniques and is shown in Fig. 2. Overall, the synthesis of the biosensor is based on the following four steps: A) electrochemical activation of the C-SPE; B) immobilization of the CNT-PAH /Ptd on the biosensor surface; C) electropolymerization of the MIP and NIP materials; and D) removal of STEAP1 (Fig. 1). The analysis of the different electrochemical steps is shown by EIS (Fig. 2A) and CV (Fig. 2B).

The polymer was electrodeposited by CV for ten consecutive cycles at a scan rate of 0.02 V/s. Preferably, at a scan rate of 0.02 V/s, a lower current can flow in the reaction and the polymerization rate can be controlled to deposit the same quality of pyrrole-2-carboxylic acid film on each electrode. Fig. S1 shows the scan of the 1st cycle of the film that started with the formation of the free radical, when a reduction peak was observed at a potential of about − 0.30 V and an oxidation peak near 1.0 V. The film was deposited at the same rate as the free radical. The deposition of the film started in the 1st cycle of the film.

As the number of cycles increased, the reduction peak at − 0.3 V disappeared, indicating the formation of an irreversible reaction probably due to the presence of a polymer. The peak current gradually decreases from the 1st cycle to the 5th cycle at about 1.0 V and then increases to the 10th cycle. This observation indicates that there is an equilibrium between the insulating and conducting layers. Overall, the peak current decreases till the 5th cycle at about 1.0 V, indicating the presence of an insulating layer. However, the film deposited after the 5th cycle appears to be conductive once the current begins to increase. Thus, the final polymer exhibits insulating properties and is not electroactive once EIS and CV measurements with a redox demonstrate the presence of an insulating material (Fig. 2).

According to the EIS spectra shown in Fig. 2A, a relevant decrease in the semicircle diameter (Rct) of the Nyquist plot was observed after modification of the C-SPE with the CNT-PAH /Ptd nanocomposite. This behavior was expected since this material with platinum and CNT is a very conductive material [24,26]. Another advantage of this nanomaterial is the presence of amino groups that interact with the carboxyl groups of the monomers and protein through electrostatic and hydrogen bonding, which contributes to the formation of a more stable polymer.

Electropolymerization of the materials MIP and NIP was performed using the CV technique. First, the potential range was set to − 0.8 to 1.1 V because the oxidation peak of PY-COOH is at 0.9 V. Then, the scan rate was optimized to obtain a more stable polymeric network. For this purpose, scan rates of 0.02 and 0.05 V/s were tested. The scan rate chosen was 0.02 V/s, as this is the only condition that ensures molecular

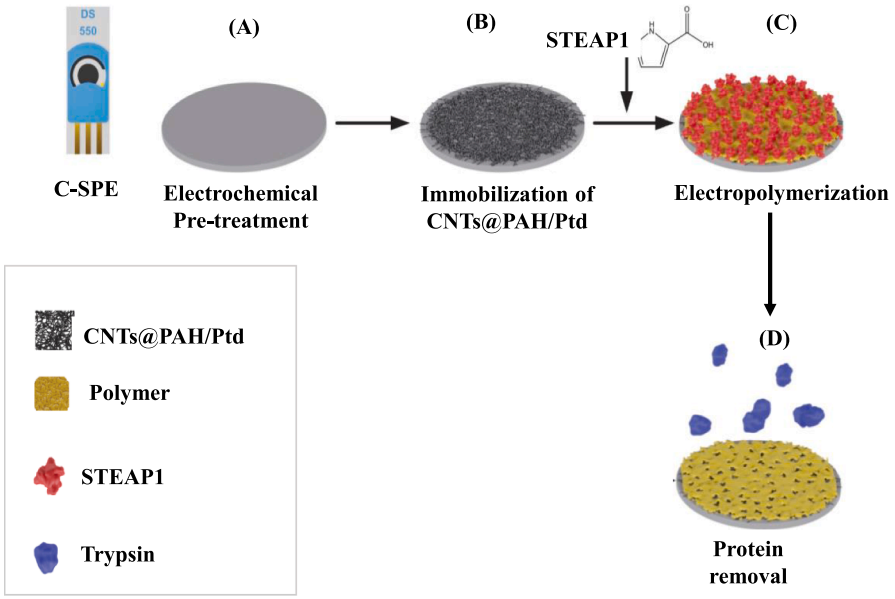

Fig. 1. Schematic illustrating the different steps in the construction of an electrochemical biosensor based on a molecularly imprinted polymer for the detection of STEAP1 protein.

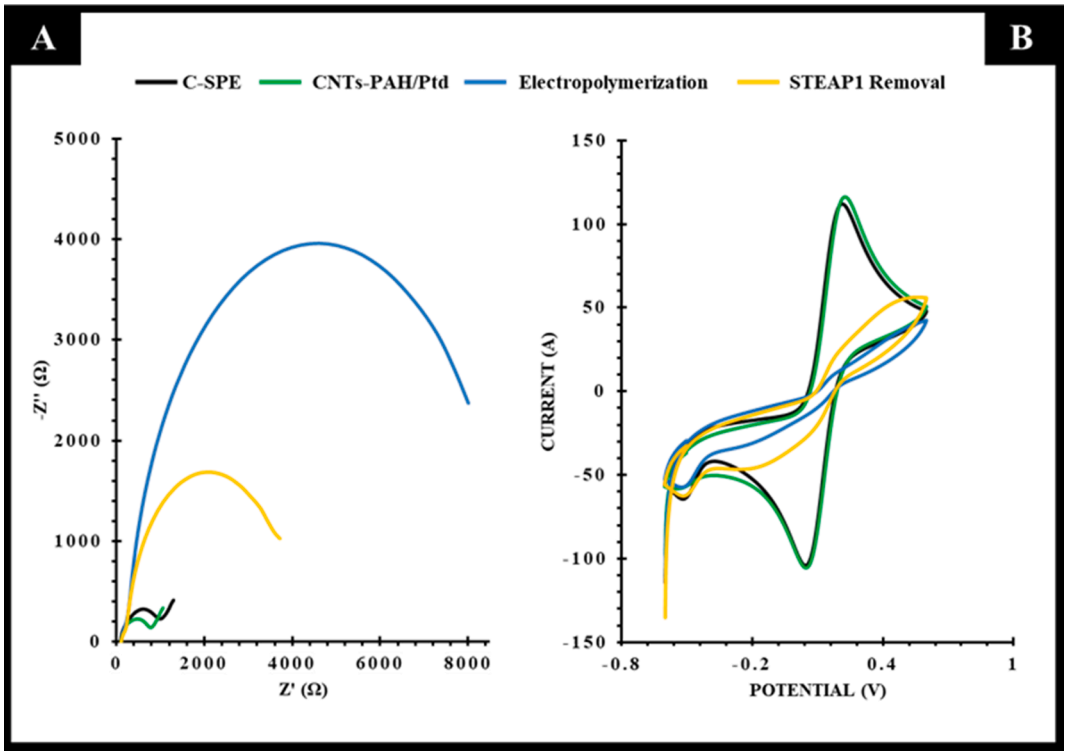

Fig. 2. Electrochemical follow-up of the electrode's modification. (A) results of the EIS technique of the sensor before any modification (C-SPE) (black), after immobilization of the CNTs-PAH/Ptd (green), after electropolymerization (blue), and after STEAP1 removal via trypsin (yellow). In (B) are present the results of the CV technique for the different steps represented in (A).

imprinting of the protein based on the pore sizes formed (Fig. S2), as shown by the linearity of the calibration curve (Fig. S3). After the imprinting phase, a huge increase in Rct was observed, indicating an insulating material compatible with the electrochemical conditions and pH of electropolymerization (overoxidation of the polymer and physiological pH). Next, the template was removed from the polymer matrix. This step is important because it leads to cavities that have the shape of the protein. It is also relevant to highlight that this procedure should not chemically change the polymer surface. Different methods such as oxalic acid, proteinase and trypsin were tested (Fig. S3). However, the sensor surface was only stabilized by treatment with trypsin at physiological pH and was therefore selected as the method for protein extraction. Specifically, 100-fold diluted trypsin was used as the removal agent. 5 μl were added to the working electrode and incubated at 37 °C for 1 h.

In Fig. 2A, after enzymatic removal of STEAP1 with trypsin, a decrease in resistance to current flow can be seen, which is due to the cavities formed on the surface that facilitate electron transfer. Since the protein has a moderate molecular weight and the removal agent also acts on the polymeric network, it is expected that after removal, the cavities in the polymeric network facilitate electron transfer and decrease the resistance to current flow.

The CV measurements are consistent with the EIS data. After electrode modification with the CNT-PAH /Ptd nanocomposite, a slight increase in net current was observed (Fig. 2B). Then, after electropolymerization, a decrease in net current was detected and the oxidation and reduction peaks almost disappeared. This behavior is consistent with a highly insulating polymer as described by Manuela F. Frasco and coworkers [27]. After removal of the template, an increase in the net current was observed, which can be attributed to the presence of cavities. Overall, these results confirm the electrochemical modification of the electrodes.

3.2. Physicochemical characterization of the biosensor

3.2.1. Raman spectroscopy

Raman spectroscopy is a high-resolution technique that can quickly provide chemical and structural information about a material. In this way, through a 532 nm laser it's possible to distinguish different stages of the electrode modification such as: (A) C-SPE without modification, (B) C-SPE functionalized with CNTs-PAH-Pt, (C) NIP without STEAP1, (D) MIP with STEAP1 removal and (E) MIP without STEAP1 removal. Then, the different modifications can be proven by analyzing the ID/IG index.

Analysing the general structure of the spectrum (Fig. 3), two very clear peaks appear. The first peak is located in the region around 1300 cm^{-1} (D-band) and the second in the region around 1600 (G-band) cm^{-1}. In addition, the intensity ratio between peaks D and G is also shown, which is particularly useful to determine the purity and degree of chemical alteration of each sample. In this way, significant differences in intensity and peak shift between different materials can be identified. Comparing the presence and shift of the bands between C-SPE and C-SPE functionalized with CNTs - PAH /Ptd, with ID/IG index values of 0.772 and 0.725, respectively, this decrease is due to the presence of a decrease in the structural defects of the sample due to the presence of CNTs in the composite material which occurs because the carbon nanotubes used were produced in absence of oxygen, so the most of the structure was preserved and the defects decreased. As for the Raman spectra of MIP before the removal of the protein and of MIP after the removal of the template from the polymer, the most relevant output is the ratio of their peaks. ID/IG ratios of 0.844 and 0.752 indicate that the defects decreased due to the removal of the protein from the matrix. This suggests that the protein affects the surface of the biosensor by introducing disorder into the structure of the material. In general, these results confirm the occurrence of chemical modifications in the electrode, and it is possible to distinguish the different modification steps.

3.2.2. Surface electron microscopy (SEM)

SEM is an important tool for the morphological analysis of materials and can produce three-dimensional, high-resolution images. For this purpose, the different nanomaterials were analyzed to distinguish the different modifications on the sensor surface. These include: (i) the C-SPE modified with the CNTs-PAH /Pt nanocomposite; (ii) MIP with template removal; and (iii) NIP (Fig. 4).

It is obvious that the CNTs are modified with PAH and dendritic Pt on the electrode surface. In the 50,000× magnification image, the surface of the CNTs densely coated with Pt nanoparticles can be clearly seen. When the C-SPE CNTs-PAH /Pt are modified with the MIP and NIP material, an increase in the thickness of the carbon rods is observed and the surface becomes opaque. For the NIP material, the presence of a polymer film in the modified C-SPE is more evident once we could not observe carbon nanotubes on the image. This is expected when the NIP has no cavities. In addition, the conductivity of the biomaterial was significantly reduced. This was evident from the poor resolution of the SEM image of MIP and NIP materials at 50,000× magnification.

3.3. Evaluation of the analytical performance of the biosensor

3.3.1. Calibration curve in buffer

After the synthesis and characterization of the biosensor, the next step is to evaluate its ability to detect STEAP1, i.e., the ability of the MIP to detect the protein through the mold cavities created after STEAP1 removal from the polymer matrix by enzymatic treatment. Calibration

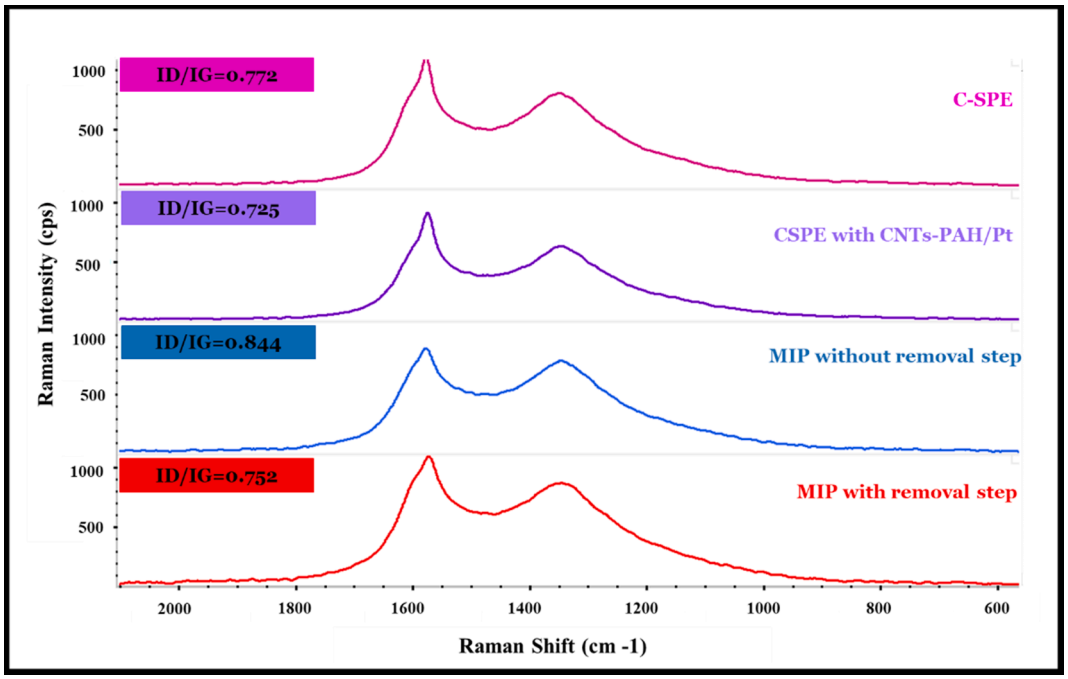

Fig. 3. Raman spectra for different immobilization steps.

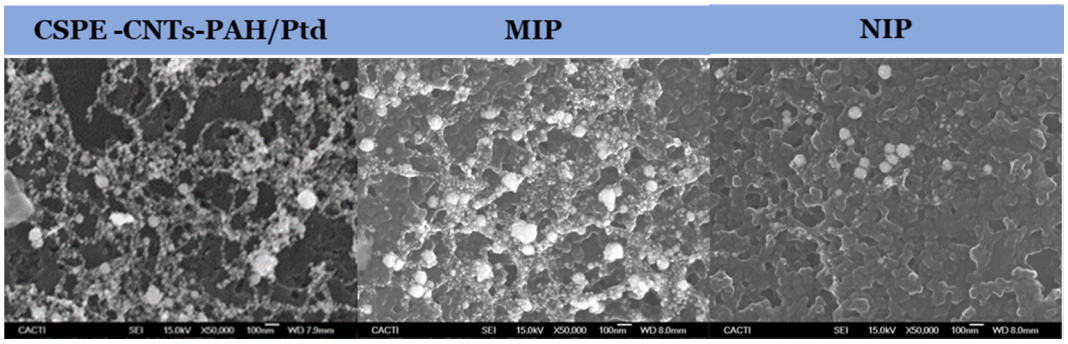

Fig. 4. Results regarding SEM analysis of different sensor materials at a magnification of 50,000 ×.

curves were generated for the electrodes modified with and without nanocomposite.

The analytical performance of the biosensor starts with the calibration of the sensors in PBS buffer at physiological pH and is represented by the relationship between the analyte concentration and the measured signal, as shown in Fig. 5. For this purpose, the sensors were incubated with 5 µl of standard STEAP1 solutions diluted in PBS with different concentrations from 0.00013 to 13 µg/ml, starting with the lowest concentration. Then, after each incubation and using the SWV technique, measurements were performed with the redox solution (Fig. 5A). The calibration curves of the MIP and NIP sensors are shown in Fig. 5B. All measurements were performed in triplicate.

Fig. 5A shows a proportional increase in current with increasing STEAP1 concentration, demonstrating that the biosensor can discriminate different protein concentrations. This increase in current with increasing STEAP1 concentration was probably related to the positive protonation of the imprinted surface due to the interaction of STEAP1 with the carboxyl groups of the imprinted polymers under the conditions in which the test was performed. While, the isoelectric point (PI) of the STEAP1 protein is 9.28, which is higher than the pH of the buffer medium of 7.4. [28]. If the PI is higher than the pH, it means that the protein is positively charged. Such an interaction between STEAP1 and MIP increases the density of positive charges on the receptor surface, which in turn increases the number of negatively charged iron redox probe molecules attracted to the surface.This behavior was also observed in the work related by M. de L. Gonçalves and coworkers [21].

In Fig. 5B, MIP showed a better slope value 0.8219 µA/ ([log, [sSTEAP1,] µg/mL), indicating higher sensitivity, and a higher R^2 value (0.995) compared with NIP (slope of 0.5581 µA/([log, [STEAP1,] µg/mL), and R^2 of 0.9486). It can be concluded that the biosensor can detect and discriminate STEAP1 at different concentrations and that the molecular imprinting technique is beneficial for the analytical performance of the biosensor, as MIP showed better results than NIP. As for the analytical performance of the sensor without the presence of the nanocomposite, no linear response was obtained, which means that the nanocomposite is essential for the detection of the protein by the imprinting sites of the MIP sensor. (See Fig. S4).

3.3.2. *Calibration curve in pellet of LNCaP cellular extracts*

To understand the behavior of STEAP1 in a more complex sample, the calibration curve for the MIP sensor was evaluated in a spiked LNCaP cell extract (Fig. 6) which contains other molecules that could interfere with the main detection step. Standards were prepared according to the procedure described in Section 3.2.1, except that dilution of the protein

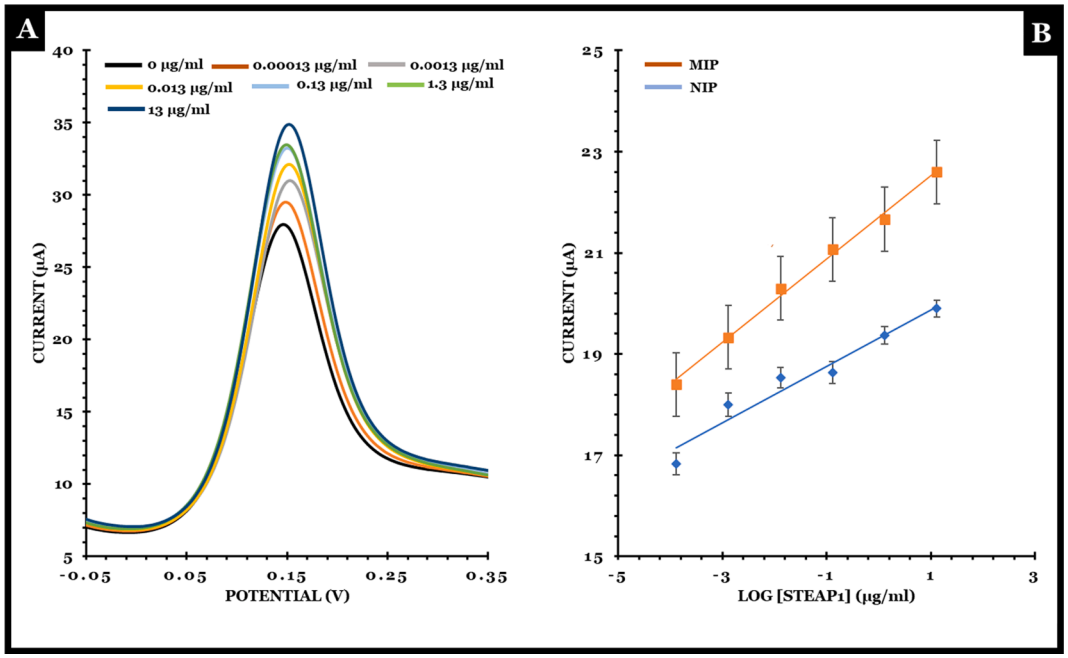

Fig. 5. Results for calibration with the different standards using trypsin at physiological pH as a removal agent. In (A) is the plot of the SWV corresponding to the calibration in PBS of a MIP. In (B) are the calibration lines with the respective error bars of triplicates of MIP ($Y = 0.8219x + 21.7$; $R^2 = 0.995$) and NIP ($Y = 0.5581X + 19.318$; $R^2 = 0.9486$).

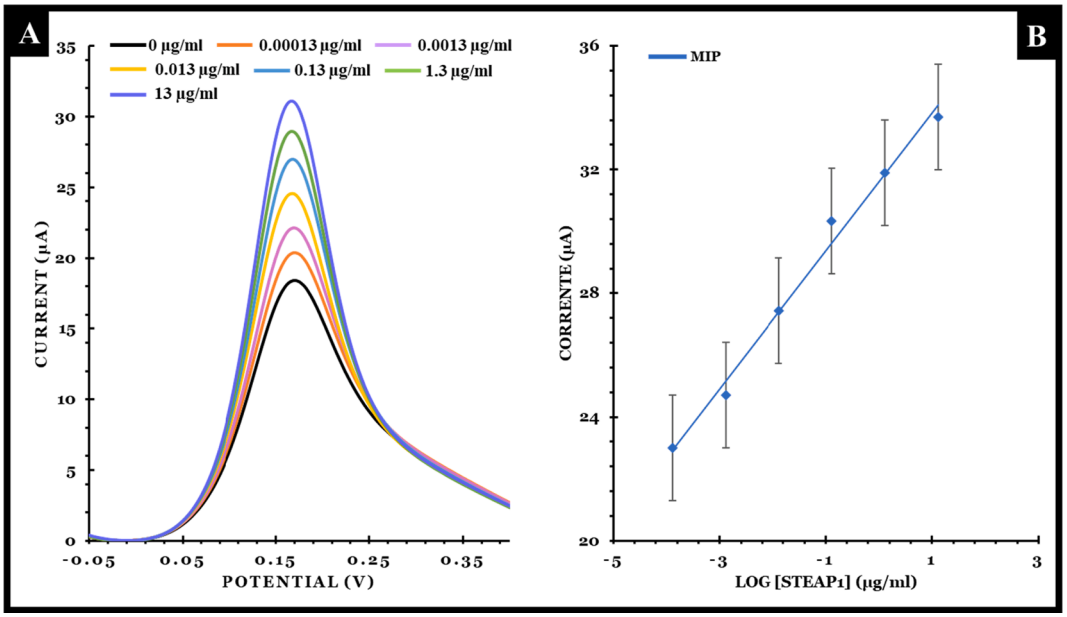

Fig. 6. Calibration results with different STEAP1 standards ranging from 0 to 13 µg/ml were prepared in cell extract from LNCaP cell culture medium. (A) result related to the SWV technique. (B) Calibration straight line of triplicates of MIP (Y = 2.2286x + 31.6; R^2 = *0.99)*.

was performed to the different concentrations in the pellet of LNCaP cell extracts. Incubations were performed under the same conditions (5 µl for 20 min on the surface of the working electrode), always followed by a reading with the *redox* solution. Then, the calibration curve was generated by the SWV technique, using a series of points obtained by incubation with the different standards.

In Fig. 6A, the increased signal in the response is proportional to the increase in STEAP1 concentration in the different standards. Fig. 6B shows the calibration line of the triplicate MIPs and it can be seen the high linearity of the signal by the high R^2 value of 0.99 and the slope 2.2286 (µA/[log, [STEAP1,] µg/mL), which also demonstrates the high sensitivity of the sensor material for the detection of STEAP1, in this case in a more complex medium. It can be concluded that the biosensor can discriminate STEAP1 in a complex medium and has high linearity and sensitivity for the response. In parallel, the same assay was performed in triplicate with NIPs that did not show linearity in response.

3.3.3. *Selectivity study*

The selectivity study was performed using the SWV technique, in which various potentially interfering species were incubated in a mixture with a specific concentration of STEAP1. Two of the interfering species were selected considering the composition of the cell extract of the culture medium of LNCaP cells, namely aminobenzoic acid (at a concentration of 1 µg/ml) and L-glutamic acid (at a concentration of 20 µg/ml) [29]. CEA protein was chosen as another interfering species (at a concentration of 0.00025 µg/ml, which corresponds to the physiological detection limit in serum samples), which is also associated with various cancers [30]. All species were diluted 10-fold, as was done for the pellet of LNCaP cell extracts. For the experimental procedure, a study of selectivity by mixing solutions was performed, i.e., two biosensors (MIPs) were used. For one of them, after stabilization in PBS, the standard 3 (0.013 µg/ml STEAP1) prepared in PBS was incubated for 20 min and then read with the iron redox solution.

From the analysis of Fig. 7, aminobenzoic acid was the interfering species with the greatest impact on the biosensor surface, with a 14% deviation from the STEAP1 signal. In contrast, L-glutamic acid was the interfering factor with the least influence on the biosensor surface change. However, all the interfering factors tested showed a deviation within the acceptable limit.

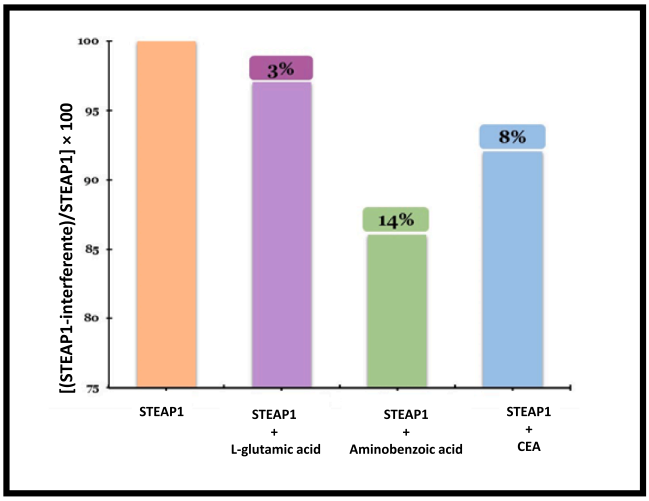

Fig. 7. Selectivity tests performed for different interfering species. L-glutamic acid, aminobenzoic acid and CEA at a concentration of 2 ug/ml, 0.1 ug/ml, 0.00025 µg/ml, respectively.

4. Conclusions

The present work focused on the development of an electrochemical biosensor for the detection of STEAP1 involving MIP and a conductive composite of CNTs PAH /Pt. To develop the sensor material, an electropolymerization step of a mixture of STEAP1 and monomer (PY-COOH) was performed. Then, for molecular imprinting of the protein, an enzymatic removal step was performed using trypsin, resulting in template voids representative of a MIP material. Additionally, the biosensor developed in this work showed good characteristics in terms of selectivity, sensitivity and reproducibility, and was characterized by low measurement time and high linearity in detection, indicating good analytical performance in STEAP1 detection. Although the definition of the physiological limit of STEAP1 in still under investigations, the biosensor presented in this work is ready for the improvements needed for its commercialization in the pharmaceutical field.

Declaration of Competing Interest

The authors declare that they have no known competing financial interests or personal relationships that could have appeared to influence the work reported in this paper.

Data availability

The data that has been used is confidential.

Acknowledgments

Rui S. Gomes acknowledge is PhD in Doctoral Program in Biomedical Engineering (PRODEB) from Faculty of Engineering, Porto University

The authors acknowledge the support from by the Health Sciences Research Centre CICS-UBI (UIDB/00709/2020 and UIDP/00709/2020), the Applied Molecular Biosciences Unit UCIBIO (UIDB/04378/2020 and UIDP/04378/2020) and the Associate Laboratory Institute for Health and Bioeconomy–i4HB (project LA/P/0140/2020) which are financed by National Funds from FCT/MCTES. Jorge Barroca-Ferreira's individual PhD FCT Fellowship (SFRH/BD/130068/2017)

Appendix A. Supplementary material

Supplementary data to this article can be found online at https://doi.org/10.1016/j.bioelechem.2023.108461.

References

[1] Y. Bhanji, W.B. Isaacs, J. Xu, K.A. Cooney, Prostate cancer predisposition, Urol. Clin. North Am. 48 (3) (2021) 283–296, https://doi.org/10.1016/j.ucl.2021.03.001.

[2] K. Rajagopalan, S.M. Mooney, N. Parekh, R.H. Getzenberg, P. Kulkarni, A majority of the cancer/testis antigens are intrinsically disordered proteins, J. Cell. Biochem. 112 (11) (2011) 3256–3267, https://doi.org/10.1002/jcb.23252.

[3] D.A. Chistiakov, V.A. Myasoedova, A.V. Grechko, A.A. Melnichenko, A.N. Orekhov, New biomarkers for diagnosis and prognosis of localized prostate cancer, Semin. Cancer Biol. 52 (January) (2018) 9–16, https://doi.org/10.1016/j.semcancer.2018.01.012.

[4] S.M. Rocha, J. Barroca-Ferreira, L.A. Passarinha, S. Socorro, C.J. Maia, The usefulness of STEAP proteins in prostate cancer clinical practice, in: Prostate Cancer, no. June, Exon Publications, 2021, pp. 139–154.

[5] I. M. Gomes, C.J. Maia, C.R. Santos, STEAP proteins: from structure to applications in cancer therapy, Mol. Cancer Res. 10 (5) (2012) 573–587, doi: 10.1158/1541-7786.MCR-11-0281.

[6] S.E.A. Burnell, S. Spencer-Harty, S. Howarth, O. Bodger, H. Kynaston, C. Morgan, S. H. Doak, MOHAMMAD Saleem, Utilisation of the STEAP protein family in a diagnostic setting may provide a more comprehensive prognosis of prostate cancer, PLoS One 14 (8) (2019) e0220456.

[7] I.M. Gomes, S.M. Rocha, C. Gaspar, M.I. Alvelos, C.R. Santos, S. Socorro, C.J. Maia, Knockdown of STEAP1 inhibits cell growth and induces apoptosis in LNCaP prostate cancer cells counteracting the effect of androgens, Med. Oncol. 35 (3) (2018), https://doi.org/10.1007/s12032-018-1100-0.

[8] T. Yamamoto, Y. Tamura, J.-I. Kobayashi, K. Kamiguchi, Y. Hirohashi, A. Miyazaki, T. Torigoe, H. Asanuma, H. Hiratsuka, N. Sato, Six-transmembrane epithelial antigen of the prostate-1 plays a role for in vivo tumor growth via intercellular communication, Exp. Cell Res. 319 (17) (2013) 2617–2626.

[9] J. Barroca-Ferreira, J.P. Pais, M.M. Santos, A.M. Goncalves, I.M. Gomes, I. Sousa, S. M. Rocha, L.A. Passarinha, C.J. Maia, Targeting STEAP1 protein in human cancer: current trends and future challenges, Curr. Cancer Drug Targets 18 (3) (2018) 222–230.

[10] I.M. Gomes, P. Arinto, C. Lopes, C.R. Santos, C.J. Maia, STEAP1 is overexpressed in prostate cancer and prostatic intraepithelial neoplasia lesions, and it is positively associated with Gleason score, Urol. Oncol. Semin. Orig. Investig. 32 (1) (2014) 53.e23–53.e29, https://doi.org/10.1016/j.urolonc.2013.08.028.

[11] S.M. Rocha, S. Socorro, L.A. Passarinha, C.J. Maia, Comprehensive landscape of STEAP family members expression in human cancers: unraveling the potential usefulness in clinical practice using integrated bioinformatics analysis, Data 7 (5) (2022) 64, https://doi.org/10.3390/data7050064.

[12] D.C. Danila, R.Z. Szmulewitz, U. Vaishampayan, C.S. Higano, A.D. Baron, H. N. Gilbert, F. Brunstein, M. Milojic-Blair, B. Wang, O. Kabbarah, M. Mamounas, B. M. Fine, D.J. Maslyar, A. Ungewickell, H.I. Scher, Phase I Study of DSTP3086S, an antibody-drug conjugate targeting six-transmembrane epithelial antigen of prostate 1, in metastatic castration-resistant prostate cancer, J. Clin. Oncol. 37 (36) (2019) 3518–3527.

[13] X. Xue, B.X. Bredell, E.R. Anderson, A. Martin, C. Mays, H. Nagao-Kitamoto, S. Huang, B. Győrffy, J.K. Greenson, K. Hardiman, J.R. Spence, N. Kamada, Y. M. Shah, Quantitative proteomics identifies STEAP4 as a critical regulator of mitochondrial dysfunction linking inflammation and colon cancer, Proc. Natl. Acad. Sci. 114 (45) (2017), https://doi.org/10.1073/pnas.1712946114.

[14] S. Mousa, Biosensors: the new wave in cancer diagnosis, Nanotechnol. Sci. Appl. 4 (1) (2010) 1, https://doi.org/10.2147/NSA.S13465.

[15] H.D. Jang, S.K. Kim, H. Chang, J.-W. Choi, 3D label-free prostate specific antigen (PSA) immunosensor based on graphene–gold composites, Biosens. Bioelectron. 63 (2015) 546–551, https://doi.org/10.1016/j.bios.2014.08.008.

[16] Y. Saylan, S. Akgönüllü, H. Yavuz, S. Ünal, A. Denizli, Molecularly imprinted polymer based sensors for medical applications, Sensors 19 (6) (2019) 1279, https://doi.org/10.3390/s19061279.

[17] M.A. Morales, J.M. Halpern, Guide to selecting a biorecognition element for biosensors, Bioconjug. Chem. 29 (10) (2018) 3231–3239, https://doi.org/10.1021/acs.bioconjchem.8b00592.

[18] P. Rebelo, E. Costa-Rama, I. Seguro, J.G. Pacheco, H.P.A. Nouws, M.N.D. S. Cordeiro, C. Delerue-Matos, Molecularly imprinted polymer-based electrochemical sensors for environmental analysis, Biosens. Bioelectron. 172 (2021) 112719, https://doi.org/10.1016/j.bios.2020.112719.

[19] P. Bhattarai, S. Hameed, Basics of Biosensors and Nanobiosensors, in: Nanobiosensors, Wiley, 2020, pp. 1–22.

[20] G. Sabouraud, S. Sadki, N. Brodie, The mechanisms of pyrrole electropolymerization, Chem. Soc. Rev. 29 (5) (2000) 283–293, https://doi.org/10.1039/a807124a.

[21] M.d.L. Gonçalves, L.A.N. Truta, M.G.F. Sales, F.T.C. Moreira, Electrochemical Point-of Care (PoC) determination of interleukin-6 (IL-6) using a pyrrole (Py) molecularly imprinted polymer (MIP) on a carbon-screen printed electrode (C-SPE), Anal. Lett. 54 (16) (2021) 2611–2623.

[22] R.S. Gomes, B.A. Gomez-Rodríguez, R. Fernandes, M.G.F. Sales, F.T.C. Moreira, R. F. Dutra, Plastic antibody of polypyrrole/multiwall carbon nanotubes on screen-printed electrodes for cystatin C detection, Biosensors 11 (6) (2021) 175, https://doi.org/10.3390/bios11060175.

[23] F.T.C. Moreira, M.J.M.S. Ferreira, J.R.T. Puga, M.G.F. Sales, Screen-printed electrode produced by printed-circuit board technology. Application to cancer biomarker detection by means of plastic antibody as sensing material, Sensors Actuators B Chem. 223 (2016) 927–935, https://doi.org/10.1016/j.snb.2015.09.157.

[24] P.J.F. Harris, Carbon nanotube composites, Int. Mater. Rev. 49 (1) (2004) 31–43, https://doi.org/10.1179/095066004225010505.

[25] M. Eduarda Schneider, L. Guillade, M.A. Correa-Duarte, F.T.C. Moreira, Development of a biosensor for phosphorylated Tau 181 protein detection in Early-Stage Alzheimer's disease, Bioelectrochemistry 145 (2022), 108057, https://doi.org/10.1016/j.bioelechem.2022.108057.

[26] R. Andrews, M. Weisenberger, Carbon nanotube polymer composites, Curr. Opin. Solid State Mater. Sci. 8 (1) (2004) 31–37, https://doi.org/10.1016/j.cossms.2003.10.006.

[27] M. Frasco, L. Truta, M. Sales, F. Moreira, Imprinting technology in electrochemical biomimetic sensors, Sensors 17 (3) (2017) 523, https://doi.org/10.3390/s17030523.

[28] M. Elshiaty, H. Schindler, P. Christopoulos, Principles and current clinical landscape of multispecific antibodies against cancer, Int. J. Mol. Sci. 22 (11) (2021) 5632, https://doi.org/10.3390/ijms22115632.

[29] "ThermoFisher Scientific 'Technical Resources 1187-RPMI 1640'.

[30] B.-K. Ahn, Individualized cutoff value of the serum carcinoembryonic antigen level according to TNM stage in colorectal cancer, Ann. Coloproctol. 29 (3) (2013) 91, https://doi.org/10.3393/ac.2013.29.3.91.